# Rheology and Friction of Compressed Polymer Layers Adsorbed on Solid Surfaces

Jean-Marie Georges, André Tonck, Jean-Luc Loubet, Denis Mazuyer, Etienne Georges, François Sidoroff

# Rheology and Friction of Compressed Polymer Layers Adsorbed on Solid Surfaces

Jean-Marie Georges, André Tonck, Jean-Luc Loubet, Denis Mazuyer, Etienne Georges and François Sidoroff

Laboratoire de Tribologie et de Dynamique des Systèmes(*), Ecole Centrale de Lyon, 69131 Ecully Cedex, France

*(Received 9 June 1995, received in final form 29 September 1995, accepted 3 October 1995)*

PACS.81.40Pq – Friction, lubrication, and wear
PACS.83.50Lh – Interfacial and free surface flows; slip

**Abstract.** — The rheology and the friction of adsorbed layers of poly-isoprene between two cobalt surfaces were investigated with a recently developed molecular tribometer. Each poly-isoprene layer is obtained by adsorption of the polymer from a semi-dilute solution of cis 1-4 poly- isoprene in 2,4, dicyclohexyl-2-methylpentane, which is a small hydrocarbon molecule and a good solvent of the poly-isoprene at 23 °C. The aim of these experiments is the mechanical characterizations of the compressed film formed by the contact of the two adsorbed layers,under both normal approach and sliding conditions. The rheological behaviour of adsorbed layers is studied with the normal approach of a smooth sphere on a plane. An "hydrodynamic layer" is detected on each surface, whose thickness is smaller than the thickness of each polymer layer adsorbed on the cobalt surface. During the compression process, the solvent molecules are repelled from the polymer network. When the separation distance becomes very small, the layers are formed by a compressed polymer "mesh" not connected. The mean "mesh" size is lower than the one corresponding to the "rubber" plateau of a poly-isoprene melt. During friction testing, the film thickness was accurately measured by variations of the sphere-plane capacitance. The film thickness variations follow those of the friction force and is the sum of two contributions. One is a thickness decrease due to creep of the layers themselves. Another is a very small increase of the interfacial thickness between the two layers, which was found to be dependent of the sliding speed. A "pinning" regime, where the application of a shear results in ordered polymer chains and reduced friction, is found for high pressure and low speed. The "pinning" regime corresponds to the macroscopic "static" friction regime.

## 1. Introduction

The shear properties of surfaces coated with adsorbed polymers control not only phenomena such as colloidal stability, fluid flow near the surface, but also tribological properties of solids [1]. Thus, polymer-modified lubricants have been used extensively as engine oils since the 1950's, because the main role of the polymer is to increase viscosity and thus lubricant film thickness [2]. Surfaces, covered with adsorbed polymer, can bear the contact of two solid surfaces, as shown in comprehensive experimental [3,4] and theoretical [5,6] studies conducted over the past decade.

(*) U.R.A. C.N.R.S 855

However, little is known about the shear behaviour of such layers [7], due to experimental difficulty of carrying out both normal and shear characterization of such layers.

Nevertheless, a better understanding of mechanisms of adhesion and friction is now possible with the recent development of new instruments such as the surface force apparatus, the molecular tribometer [8–12], the atomic force microscope [13–15], which make it feasible to measure, at a molecular scale, the normal and tangential forces between two surfaces. In the absence of ploughing friction due to the solid asperities, the frictional force between two smooth solids arises from adhesive bonding and hence from the mechanical shear strength of the sliding interface. The molecularly thin film of "simple" molecules or polymer melts present in the interface controls the "interfacial" friction [10], gives viscous or frictional forces [8], and can be partly simulated [16].

When the tangential compliance of the tribometer is not too low [12], stick-slip has been observed, whenever adhesion exists between the surfaces [8, 11]. With this respect, small molecules, which can form quasi-discrete layers, were used. The short range force curves characterizes an adhesive minima located at separation distances at which sliding occurs. Friction variations were explained by a "cobblestone" model, that takes into account the energy expended to overcome the intermolecular forces between the molecules, when they are dragged over each other [11, 16]. In this model, the presence of an attractive force is explicit. In the contrary, if two surfaces interact across a well adsorbed polymer film, the intersurface forces are, as in the case for the experiments presented in this paper, purely repulsive [3, 21]. Since interfacial adhesion is absent, stick-slip is not observed. The interesting aspect of sliding experiments with long chain polymer molecules is also the possibility of orientation of the molecules by the applied shear force. In the presence of such shear force, long chains molecules will become preferentially aligned in the sliding direction, and evidence for shear-induced orientation has been observed in number previous experiments [36–38]. For instance, Hirz *et al.* [36], which have investigated the frictional behaviour of mica surfaces lubricated with a linear perfluoropolyether melt, attribute the decrease of the kinetic friction in comparison with the static one, to the shear-induced orientation of the polymer.

This paper is mainly concerned with both the bearing properties of adsorbed polymer layers confined between a flat and a spherical surface, and the shearing behaviour of the highly compressed layers as shown schematically in Figure 1. The two solid surfaces are each covered with an adsorbed polymer layer of thickness $L$, and are pressed against each other with a normal load $F_s$. Opposed to an applied relative speed $\dot{X}$, a tangential force is detected and related to the friction force $T$ generated along the area of contact of radius $a$ and at the boundary of the interface of thickness $D$. An understanding of the mechanisms which control the tangential force $T$, implies a knowledge of three points. *First*, the area of the contact zone is influenced by both the mechanical and adhesive properties of the solids in contact and of the interfacial film. *Second*, the viscoelastic properties of the interfacial film, which are related to its structure, influences, in particular the interfacial thickness. *Third*, the very thin shear band is where the sliding occurs. The poor definition of the position and the thickness of these shear band is an unknown key. The analysis of these three points clearly shows how it is important to fully characterise the geometrical and mechanical properties of the adsorbed films used in these experiments. These three factors can be analysed with the same instrument: the molecular tribometer.

The paper is organised as follows, in Section 2, we describe, a new molecular tribometer, that measures with great accuracy the forces and the displacements between surfaces bearing polymer layers in a liquid medium, and the nature of the materials used (solid surfaces, polymer solution). We present, in Section 3, experimental data related to the normal approach. We particularly show, that due to its structure, the adsorbed layer presents an "hydrodynamic"

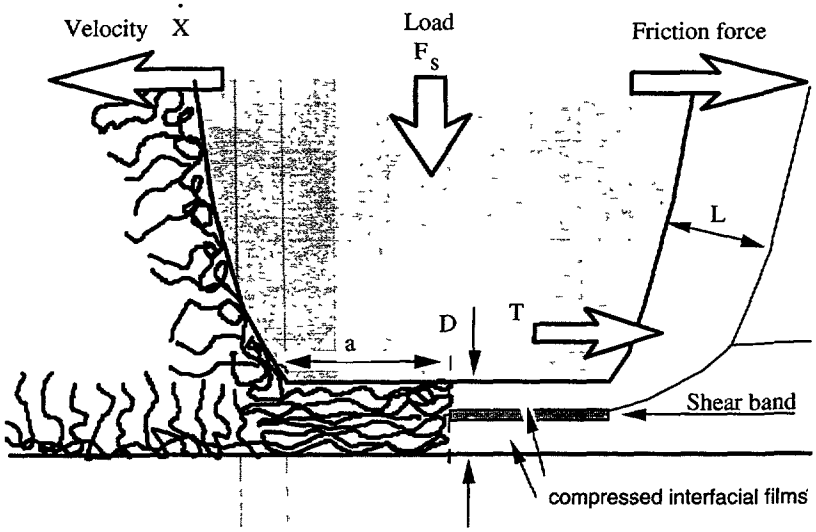


Fig. 1. — Schematic geometry of the contacting solids separated by thin compressed layers. This is also the geometry adopted in the experiments with the molecular tribometer described here. The two solid surfaces are covered with an adsorbed polymer of thickness $L$, and are pressed against each other with a normal load $F_s$. Opposed to an applied relative speed $\dot{X}$, a tangential force is detected and related to the friction force $T$ generated in the area of contact of radius a and in the interface of thickness $D$. The understanding of the mechanisms, which control the tangential force $T$, is related with the knowledge of three points: the area of the contact zone, the properties of the interfacial film, the thin shear band.

thickness $L_H$ smaller than the thickness $L$ which is determined by the static force. Finally, in Section 4, we present the sliding behaviour of the compressed layers. The measurement of the film thickness interface during the sliding process, not only detects the creep due to the shear process, but also the thickness evolution of the interpenetration zone, in which the end groups of the molecules are dragged across each other, producing the transfer of sliding energy. Technical details of the normal approach presented in Section 3, can be found in the appendix.

## 2. Experimental Methods

The purpose of these experiment are the *mechanical characterizations* of a polymer layer adsorbed on each solid surface, of the compressed film formed by the contact of two adsorbed layers, and finally *the sliding properties* of the compressed layers.

2.1. THE MOLECULAR TRIBOMETER. — A new molecular tribometer, designed for friction studies, is used in these experiments. It takes some elements of the surface force apparatus (S.F.A), previously described [17, 18].

The general principle of the molecular tribometer (Fig. 2), is that a macroscopic spherical body can be moved towards and away, in the three directions $0xyz$, from a planar one using the expansion and the vibration of a piezoelectric crystal. A sphere of radius $R$ is firmly fixed to the three axial piezoelectric translator. The plane specimen is supported by double force $(F, T)$

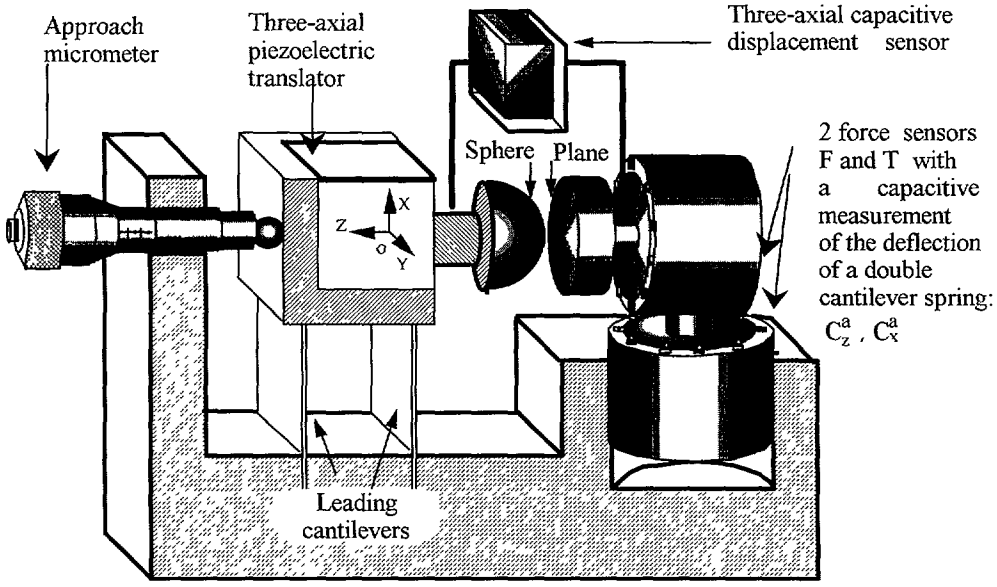


Fig. 2. — Schematic representation of a molecular tribometer, which is a surface force apparatus (S.F.A.) modified for friction studies.

sensors. Each of them is equipped with a capacitive sensor and a double cantilever spring. The sensor's high resolution allows a very low compliance to be used for the force measurement ($C_Z^a = C_X^a = 2 \times 10^{-6}$ m/N). Three sensors are designed to measure relative displacements in the three directions between supports of the two solids, with a displacement resolution of 0.01 nm in each direction.

Generally, specimens are metallic, and the electrical capacitance $C$ of the sphere-plane interface is also measured and then the sphere-plane interface closest distance $D$ detected.

Each capacitance of the capacitive sensors is determined by incorporating it in a $LC$ oscillator acting in the range 5 to 12 MHz. Each resulting frequency is measured in two ways: first by use of a frequency counter and second by use of a low noise discriminator, which directly gives a voltage function of the frequency measured.

Three feedback loops control the relative displacements between the holders of the sphere and the plane, in the three axes $oxyz$. These displacements can be automatically selected under computer control. Each displacement signal is compared with an imposed signal using a negative proportional integral (P.I.) feedback loop acting on each piezoelectric crystal via an high voltage amplifier. For instance, $X$ and $Y$ displacements can be maintained constant and the feedback process regulates the displacement $Z$ between the sphere and the plane outside of the contact region.

The experimental procedure was as follows. A set of solids samples (sphere and plane) are prepared for each experiment and mounted on the tribometer, then a droplet of test liquid is deposited between the two surfaces. Experiments are carried out in two steps. *First*, the sphere (radius $R$) is moved towards (or away) from a plane ($Oz$ direction). Normal squeeze and deformations of the adsorbed layers and solid surfaces are measured during the normal approach. *Second*, the sphere-plane interface is sheared, and relative displacements in the axis $ox$ produces characterisation of the sliding process with the measurement of the frictional force.

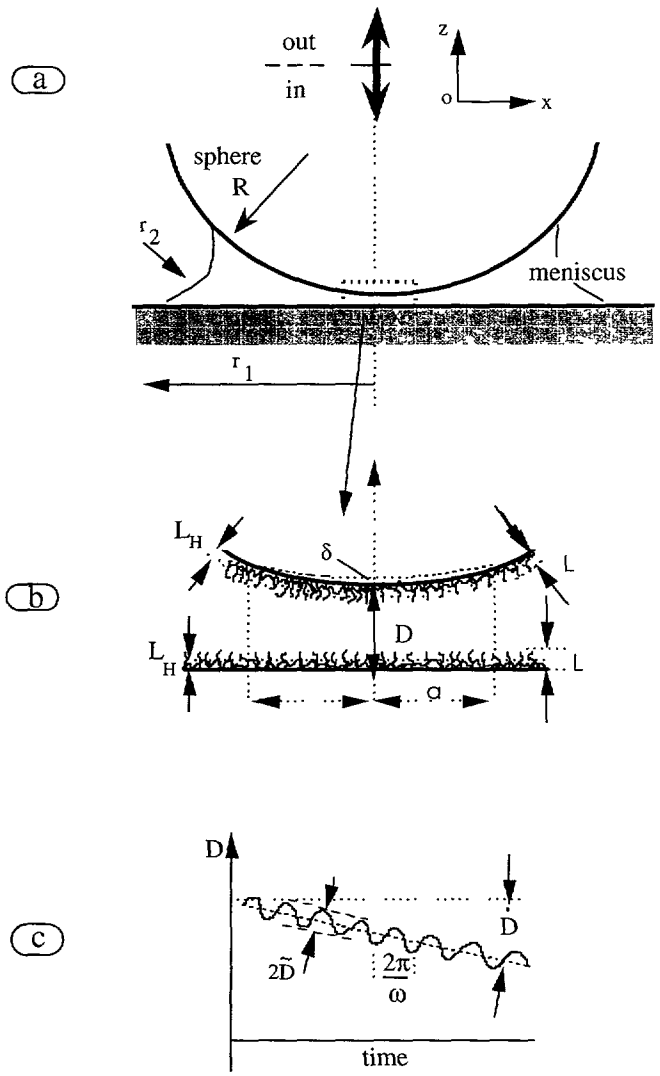


Fig. 3. — Principles of experiments in normal approach. The sphere (radius $R \approx 2$ mm) is moved towards (or away) from a plane ($oz$ direction). A meniscus of liquid is confined between sphere and plane (radii $r_1 \approx 1$ mm, and $r_2$ produces a wetting force. An adsorbed layer of polymer is obtained on each surface. Their thicknesses are $L$. $L_H$ is their "hydrodynamic" thickness . In the normal approach, the sphere-plane displacement $Z$ is monitored in order to simultaneously determine both the real separation $\overline{D}$ of the sphere and plane, and the extent of solid deformations $\delta$. The two components of the sphere-plane approach permit the analysis of the two normal forces components: dynamic $F_H$ and quasi-static $F_s$ contributions.

For the normal squeeze, in the inward and outward normal approach (Fig. 3), the sphere-plane displacement $Z$ is monitored with two speed components. One is a steady ramp, which gives a constant approach speed of 0.1 nm/s. A small amplitude oscillatory motion of about 0.1 nm RMS is superimposed on the steady motion, with a vibration period of $2.5 \times 10^{-2}$ s. The following measurements are simultaneously recorded: the sphere-plane capacitance $C$,

the "quasi-static" normal force $F_s$, and the mechanical "normal" transfer function. From this complex transfer function, only the imaginary part will be used in this paper. This component, which is the dynamic force in quadrature with respect to the oscillatory motion, gives the damping function $1/A$:

$$\frac{1}{A} = -\frac{D - 2L_H}{6\pi\eta R^2}. \tag{1}$$

where $\eta$ is the viscosity of the fluid (see appendix).

Experiments were performed in dry air in the presence of the drying agent $P_2O_5$. The temperature was 23 °C. The stabilisation time for adsorption requires between a few minutes for the pure solvent to some hours for the polymer solution.

### 2.2. Materials

*2.2.1. Solid Surfaces.* — The sphere used consists of metallic cobalt coatings on fused borosilicate glass, whose Poisson's ratio $\nu_1$ is 0.22 and Young's modulus $E_1$ = 65 GPa, (glass 732-01, Sovirel Corp.). The plane used consists of metallic cobalt coatings on a silicon wafer ($E_2$ = 166 GPa, $\nu_2$ = 0.23). This cobalt layer was deposited under a low argon pressure ($5 \times 10^{-6}$ Pa), using cathodic sputtering. Atomic force microscopy (AFM) and scanning tunneling microscopy examinations of the sputtered surfaces show that, the surfaces is made of irregular connected clusters producing a gently bumpy corrugation with a "blackberry" like roughness; (peak to valley 1 nm, measured with a scan length of 1 $\mu$m). The corrugation diameter is about 50 nm. X.P.S. analysis of these surfaces confirm the presence of metallic cobalt on the glass, and show an oxide layer of thickness less than 1 nm [18]. The low amplitude of the surface roughness is therefore negligible compared with the thickness of polymer layers considered in this study.

Dust minimisation is one key to experimental success. The use of a laminar flow bench was sufficient to reduce dust when coupled with a good inspection system, such as dark field optical microscopy.

*2.2.2. Liquids.* — Experiments were carried out with pure solvent and polymer solutions. The solvent is 2,4, dicyclohexyl-2-methylpentane (DCHPM), (Santotrac 40 from Shell Research, Thornton, U.K). The solvent was purified by distillation under pure dry nitrogen. The polymer used is the cis. 1,4, poly- isoprene $(\text{-CH}_2\text{-C-}(\text{CH}_3)\text{=CH-CH}_2)_N$, designated Pi, (Polymer Laboratories). The weight average molecular weight of the liquid polymer $M_w$, measured by gel permeation chromatography is 62800, which corresponds to a monomer number $N$ = 922. The polydispersity index is 1.03. The bulk viscosity of the pure polymer is 2900 Pa s [18]. Its radius of gyration is given by the Wall relation $R_G = 0.0198\ M_w^{0.5}$ [19], is estimated to be $R_G$ = 4.96 nm. The concentration of the cis-polyisoprene in solution with DCHPM, studied here, is 9% w/w or $c = 81 \times 10^{-3}$ g/cm$^3$.

## 3. Normal Squeeze and Deformations of the Adsorbed Layers

3.1. Experiments with Pure Solvent. — In order to check the effects of the adsorbed layer created by the polymer solution, it is first necessary to study the semi-rigid hydrocarbon DCHMP, which constitutes the solvent. The "damping profile" is obtained, using equation (1)

$$\frac{6\pi R^2}{A} = \frac{D - 2L_H}{\eta} \tag{1'}$$

in the dynamic mode.

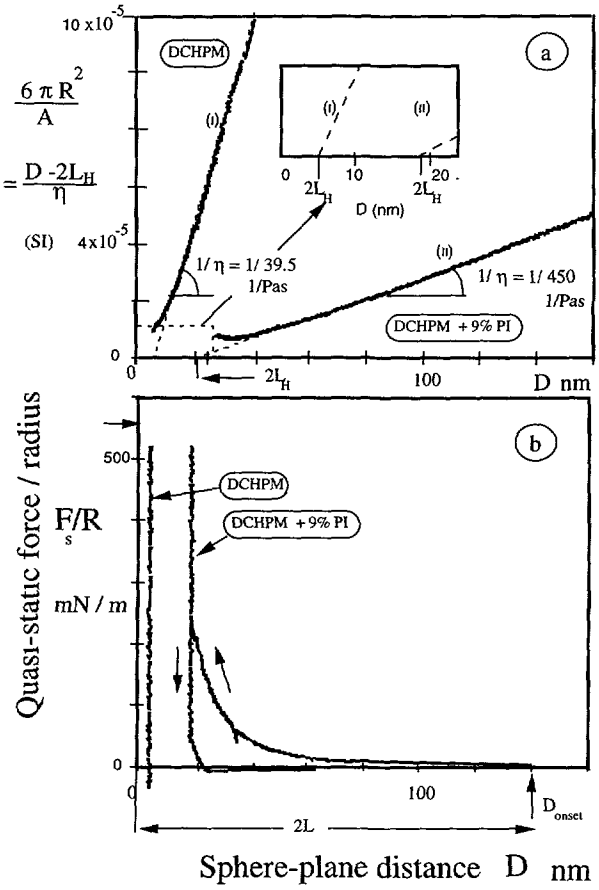


Fig. 4. — Curves a: Variations of the function $6\pi R^2/A$ with the surface separation $D$ for cobalt sphere and plane surfaces in pure 2,4, dicyclohexyl-2-methylpentane (DCHMP), and in a cis-polyisoprene solution in DCHMP (9% w/w). The straight lines corresponds respectively to a slope with $\eta_0 =$ 39.5 mPa s for DCHMP and $\eta_s = 82$ mPa s for the 9% Pis solution. The "hydrodynamic" layer are respectively $L_H = 2.5$ nm for pure DCHMP, and $L_H = 9$ nm for Pis solution. Curves b: Quasi static force ($F_s$) *versus* distance ($D$) profiles between the sphere (radius $R$) and the plane in pure DCHMP and in polyisoprene solution (9% w/w). The force profiles are normalised to yield the interaction energy per unit area in the Derjaguin approximation [21]. Repulsive interactions for the "virgin" layer (not already compressed) commence at $D_{onset} = 135 \pm 20$ nm and give a measurement of the thickness $L$ of each polymer layer adsorbed on the cobalt surface ($L = D_{onset}/2 = 68 \pm 10$ nm).

The normal force profile $F_s(D)$ in the quasi-static mode are simultaneously determined in the polymer free solvent. In Figure 4a, $6\pi R^2/A$ is plotted against the mean surface separation $D$; this reveals a linear variation, whose slope leads to the solvent viscosity $\eta_0 = 39.5 \pm 0.2$ mPa s and which intercepts the surface separation axis at $D = 2L_H = 5.0 \pm 0.2$ nm. The value of the viscosity corresponds to the literature value for bulk viscosity of DCHPM and was also checked with a capillary rheometer [23]. With the semi-rigid hydrocarbon DCHPM, a relatively thick "hydrodynamic" layer is present near the solid surfaces $L_H = 2.5 \pm 0.1$ nm, due to the conformation of the molecule, (compared with a flexible molecule such n-dodecane, where $L_H = 0.4 \pm 0.1$ nm) [18].

Figure 4b shows also, $F_s(D)/R$ plotted against closest distance $D$ between the sphere (radius $R$) and the plane. The force distance profile (Fig. 4b) has been already reported [18]. During the squeeze process, a "confined" layer appears due to molecule entanglements. The contact pressure orients molecules giving a resultant layer subsequently resistant to a relatively high compressive pressure which has a thickness of $5 \pm 0.5$ nm.

3.2. "HYDRODYNAMIC" THICKNESS OF AN ADSORBED LAYER IN POLYMER SOLUTION. — Measurements in the polyisoprene solution in DCHPM at a concentration $c = 8.1 \times 10^{-2}$ g/cm$^3$, were conducted after 30 hours of incubation. The "damping profile", in the dynamic mode and the normal force profile $F_s(D)$ in the quasi-static mode are also simultaneously determined, Figure 4.

A plot of $6\pi R^2/A$ *versus* $D$, (Fig. 4a) again reveals a linear variation similar to that of the pure solvent. The viscosity measured is $\eta_s = 450 \pm 10$ mPa s, it corresponds to the bulk viscosity of the polymer solution, since a value of $466 \pm 10$ mPa s is found for the same solution with a capillary rheometer [23]. It is possible to show that the maximum shear rate in these experiments are of the order of 1 to 10 s$^{-1}$ [18].

The bulk viscosity was measured for different concentration of the polymer solution $8 \times 10^{-4} < c < 10^{-1}$ g/cm$^3$, with capillary rheometer and SFA. The data, not reported here, give a limiting viscosity number $[\eta] = \lim_{c \to 0} \dfrac{\eta_s - \eta_0}{\eta_0 c} = 110 \pm 15$ cm$^3$/g.

Therefore the critical concentration $c^*$ at which the overlap of the polymer coils starts is estimated to be $c^* = 1/[\eta] = 9 \pm 1 \times 10^{-3}$ g/cm$^3$. In these experiments $c = 9c^*$, corresponds to the *semi-dilute regime* [20].

The hydrodynamic radius $R_H$ of the coil of polymer in the dilute regime, can be evaluated by the relation:

$$R_H^3 = 0.0955[\eta]\frac{M_w}{N_A} \tag{2}$$

where $N_A$ is the Avogadro number. Numerical application gives $R_H = 10.5 \pm 0.5$ nm. The ratio $R_H/R_G$, is considered as a criterion for the solvent quality [24], it has a value equal to 1.51 for $\theta$ solvent, and to 1.7-2.5 for good solvent; here it is found 2.2.

In the semi-dilute regime the correlation length $\zeta$ between two interpenetrated coil can be evaluated by the relation:

$$\zeta = 2R_H \left(\frac{c^*}{c}\right)^{3/4} \tag{3}$$

Numerical application gives $\zeta = 4$ nm.

*It is concluded that DCHPM, is a good solvent of the polyisoprene at* 23.5 °C, *and that the regime is semi-dilute.*

The intercept of the extrapolation of $6\pi R^2/A$ with the surface separation axis is $D = 2L_H = 18.0 \pm 0.2$ nm. This corresponds to an "hydrodynamic layer" on *each surface*, whose thickness is $L_H = 9.0 \pm 0.1$ nm.

In our experiments, the "hydrodynamic layer" $L_H = 9$ nm is founded to be such as $L_H/\zeta = 2.25$; $L_H$ appears to be comparable with the diameter of free coil, result is in good agreement with the experimental work of Cohen-Stuart *et al.* [40].

3.3. MECHANICAL BEHAVIOUR OF COMPRESSED ADSORBED LAYERS. — Figure 4b shows that repulsive interactions for the uncompressed layer start at $D_{onset} = 135 \pm 20$ nm. This can correspond to the beginning of interpenetrating adsorbed layers. The *measurement of the thickness L of each polymer layer adsorbed* on the cobalt surface gives $L = D_{onset}/2 = 68 \pm 20$ nm. This thickness is found to be larger than the "hydrodynamic" layer thickness, and

$L = 17\zeta$. This result suggests that the system is not completely in equilibrium and that the polymer molecules, even if the approach speed is small, are not expelled from the contact.

The repulsive forces created by the deformation of the compressed adsorbed layers are explained by the steric forces created by adsorbed polymer layers. Their origin are explained by Luckham and Klein [4], Sens, Marques and Joanny for adsorbed layer [6], and Fredrickson and Pincus [5] for compressed grafted polymer layers. Chains are considered as an elastic porous medium through which the solvent flows.

Here, these forces are difficult to formulate for two main reasons. (i) First, neither the amount of adsorbed polymer nor the number of binding sites per molecule are known. (ii) Second, *during the inward and outward approach* (Fig. 4b), the force distance profile shows an inelastic behaviour of the film. This irreversible behaviour is present for a time scale larger than the time scale of the experiment, which is of the order of a few minutes. We have repeated the same indentation experiment 10 hours later and found that the layer has not yet relax completely.

Furthermore, the experiment presented in Figure 4b shows that when $F_s(D)/R$ is higher than 200 mN/m, the compressed layers stays at a residual thickness of 19.3 nm which resists to the high contact pressure $p > 30$ MPa.

Furthermore, we conclude, that DCHPM molecules can flow in the polymer adsorbed layer, whose thickness is $L = 68 \pm 20$ nm, and because polymer tails only partly hinder the flow, the hydrodynamic thickness $L_H$ is smaller than $L$, ($L_H = 0.15L = 9$ nm). During the compression process DCHPM molecules are expelled from the polymer network, and especially from superficial tails; so that, when the distance separation $Z$ is less than 30 nm, the interfacial layer is mainly composed of the "rubber" polyisoprene (see 4.1).

The force-separation curves $F_s(D)/R$ from Figure 4, presents, a very low adhesion force $F_s^a/R = 0.01$ mN/m. It is known that [30], in the polymer adhesion problem, three processes have been noted: the effect of dispersive forces, chain pull-out, and chain breaking. The level of the energy measured in this experiment shows that the last two processes are not present. This suggests that the polymer chains belonging to one adsorbed layer has not enough time to diffuse into the second adsorbed layer, that the two compressed layers do not interdigitate strongly, and finally that the contact plane between the two solids are well defined.

## 4. Frictional Behaviour of Compressed Adsorbed Layers

The analysis of the behaviour in friction of highly compressed polyisoprene films can be considered, because we have a relatively good description of the interface. In the contact area, one "mesh" of polyisoprene molecules covers each solid surface in contact. The adhesion between the two "meshes" is negligible, indicating that no molecule diffuse in the opposite "mesh". Consequently, it is possible to deduce that the shear plane occurs between these two "meshes", and not between each layer and the substrate, where an irreversible adsorption is produced, or in the interior of one on the layer. Friction is studied for different sliding speeds and different contact pressures, in order to describe the friction behaviour.

4.1. Initial Friction Process of Very Compressed Films. — The sphere and the plane are pressed with *a constant normal load* during the test ($F_s = 508 \pm 1$ $\mu$N). The sphere indentation in the two adsorbed films of thickness $2L$, makes circular contact area of radius $a_f = 23$ mm. In the middle of the contact is disposed the circular Hertzian contact area of radius $a = 2.4$ mm (Fig. 5). This corresponds to cobalt-glass substrate deformations $\delta$ equal to 3.3 nm and an Hertzian pressure evaluated to 28 MPa. The tangential piezoelectric transducer permits a relative sliding displacement $X$ between the sphere and the plane. $X$ is

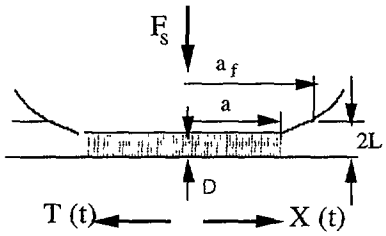


Fig. 5. — Friction of very compressed layers. The sphere and the plane are pressed with a constant normal compression ($F_s$ = 508 $\mu$N, Fig. 4). The sphere indentation in the two adsorbed films of thickness $2L$, realises a circular contact area of radius $a_f$ = 23 $\mu$m. In the middle of the contact is disposed the circular Hertzian contact area $a$ = 2.4 $\mu$m.

also measured with a resolution better than 0.01 nm. It is important to note, that all the sliding displacements, realised in the experiments reported in this paper, are small in comparison with the Hertzian contact radius.

The variations of the tangential force $T$ and those of the film thickness $\Delta D$, as measured by the electric capacitance of the sphere-plane interface, are studied as a function of time or displacement $X$. Figure 6 shows the simultaneous variations of $T$ and $\Delta D$ *versus* time, when a constant sliding speed of $\dot{X}$ = 0.2 nm/s is applied.

*(i) The Tangential Force.* — The tangential force detected is principally related to the friction force $T$ generated along the Hertzian area of contact, of thickness $D$,where pressure is high. The measured tangential compliance $\{dX/dT\}_{(D=\text{const},X=0)}$ is also assumed to be related to this area of high pressure. With this assumption, an estimation of the elastic shear modulus of the confined layer can be computed.

The measured tangential compliance is the sum of the tangential compliance of the Hertzian contact $C_X^{He}$, and of the tangential compliance of the thin film $C_X^f$ pressed in the Hertzian contact:

$$\{dX/dT\}_{(D=\text{const},X=0)} = C_X^{He} + C_X^f \tag{4}$$

Their values are respectively:

$$\{dX/dT\}_{(D=\text{const},X=0)} = 9 \times 10^{-6} \text{ m/N};$$

the normal and tangential compliances of the Hertzian contact being related [31,32]:

$$C_X^{He} = 1.15\, C_Z^{He}, \tag{5}$$

therefore $C_X^{He} = 4.6 \times 10^{-6}$ m/N.

Therefore the tangential compliance of the film can be determined with a good accuracy with the equation (6) and is $C_X^f = 4.4 \times 10^{-6}$ m/N. The shear modulus $G_f$ of the compressed films is obtained with the relation:

$$G_f = \frac{D}{\pi a^2 C_X^f}, \tag{6}$$

and found to be equal to 250 ± 30 MPa. Consequently the compressive modulus is $E_f$ = 650 ± 80 MPa, and therefore this test is conducted with a pressure ratio $p/E_f = 0.52$. According to the scaling theory of polymer [20], the shear elastic modulus of the polymer network is related

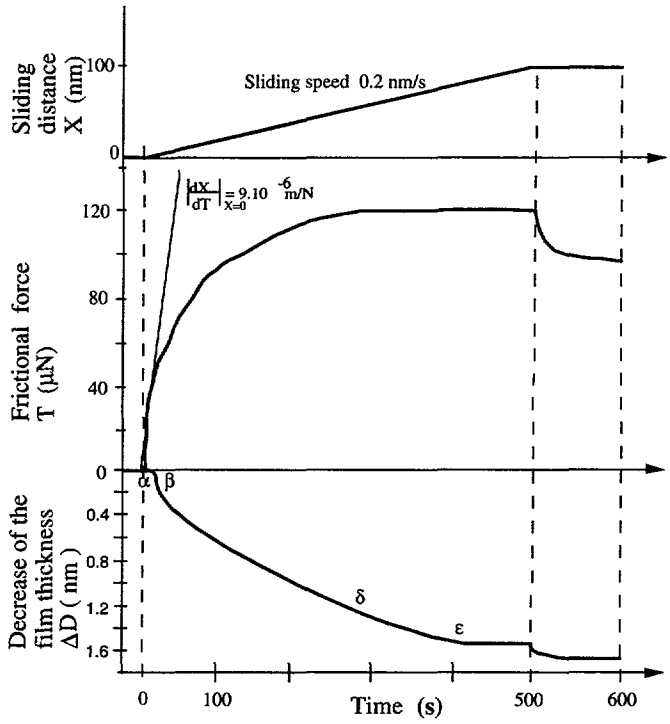


Fig. 6. — Initial friction process of very compressed layers. The tangential force detected increases non-linearly with the displacement. The film thickness, which is initially equal to $D = 19.3$ nm, decreases.

to the entanglement distance $\xi$, which is of the order of the mesh size of the temporary network formed by the chains, by the relation:

$$G_f \propto \frac{k_B T}{\xi^3} \tag{7}$$

According to Rault [29], for the cis-polyisoprene in melt $\xi = 8.2$ nm and $G_f = 0.44$ MPa; therefore, $\xi$ of the compressed polymer is evaluated to be 1 nm. Due to applied external pressure, because the polymer does not escape from the contact area, the "mesh" size of the polymer layer is reduced. We note that a value of $\xi$ is close to the DCHPM molecule size (1 nm) [18]. Therefore, in the thickness of the interface ($D = 19.3$ nm), each "mesh" layer contains between 5 to 20 polymer molecules, (20, if the polymer molecules are in contact).

At this compression rate, layers behave as a solid in the rubbery state. This result is in accordance with the literature data [41]. The glass transition temperature for pure polyisoprene is $T_g \approx -73$ °C. The constant of compressibility $dT_g/dp \approx 2.4 \times 10^{-7}$ °C/Pa. Therefore an applied pressure of 28 MPa will shift the transition temperature by 7.2 °C, and will give $T_g \approx -66$ °C. We conclude at the experiment temperature (23 °C), the glassy state is not reached, and that the friction study is therefore dominated by the behaviour of the highly compressed polyisoprene layers, which are in the rubbery state.

Figure 5 shows also that, the tangential force detected increases non-linearly with the displacement. A relative displacement evaluated between 50 to 100 nm is needed for the tangential

force to reach the "stabilised" friction force $T_L$. At this level, the shear stress of the film, assumed uniformly distributed on the indented film area, is $\tau = T_L/\pi a^2 = 7.6$ MPa, and the friction coefficient $\mu = T_L/F_s$ is found in the range of $\mu = 0.27$.

*(ii) The Decrease of the Film Thickness $\Delta D$.* — The film thickness, which is initially equal to $D = 19.3$ nm, decreases, as $X$ increases. This decrease can be followed accurately by variations of the sphere-plane capacitance $C$ or less accurately, by the measurement of the normal displacement $Z$. For this initial sliding experiment, the decrease is extended with a distance of 80 nm. When, after sliding at a speed of 0.2 nm/s, the sliding is stopped, the tangential force and the film thickness does not relax immediately and completely.

Film thickness variations follow those of the friction force variations and can be considered as the sum of two contributions $\Delta D_1$ and $\Delta D_2$, as described in Figure 6. The variations of the thickness $\Delta D_1$ are attributed to be due to the creep of the layers themselves. $\Delta D_1$ is negative and essentially dependent on the sliding distance $X$ and the normal applied pressure $p$. $\Delta D_1$ decreases, when the sliding distance $X$ increases. The variation of the thickness $\Delta D_2$ is positive and is an increase of the interface between the two layers due to the sliding speed. $\Delta D_2$ increases when the sliding speed increases. Therefore $\Delta D$ can be written as:

$$\Delta D = \Delta D_1(X, p) + \Delta D_2(\dot{X}, p).$$

4.2. Effect of the Sliding Speed. — Figure 7 shows the frictional force $T$ and fluctuations of the film thickness $\Delta D$ for the same experiment as in Figure 6, but for different sliding speeds. During the sliding process, the speed is increased by steps (0.2; 2.5; 25; and $10^5$ nm/s). The frictional force $T$ and the fluctuations of the film thickness $\Delta D$ are simultaneously found to be dependent on the sliding speed $\dot{X}$. The "stabilised" friction force $T_L$, obtained for each speed, is reached more and more rapidly, as the sliding speed increases. This suggests that the relevant parameter is not the time, but one sliding distance, evaluated between 50 to 100 nm. This distance, which is roughly of the same order than the length of the long compressed tails. We note also that $T_L$ decreases as the speed increases.

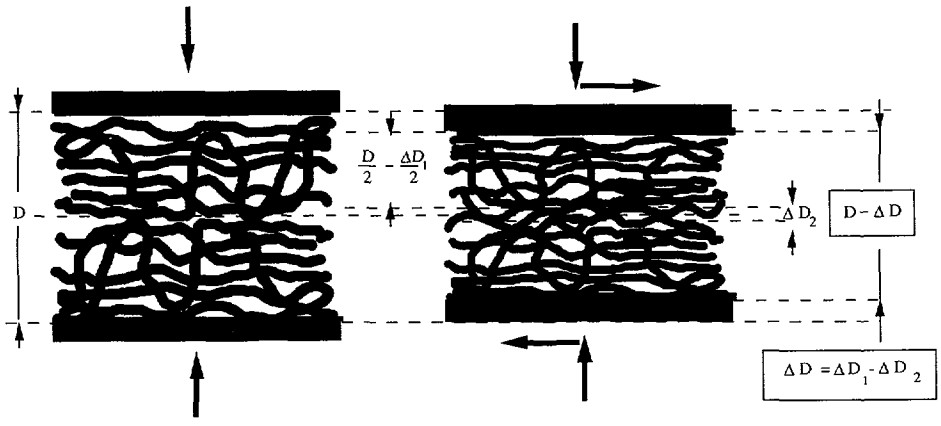


Fig. 7. — Film thickness variations are considered as the sum of two contributions $\Delta D_1$ and $\Delta D_2$. Variations of the thickness $\Delta D_1$ are attributed to the decrease of films thickness $D$, due to the creep of layers itself. $\Delta D_1$ is negative and essentially dependant of the sliding distance $X$ and of the normal applied pressure $p$. Variation of the thickness $\Delta D_2$ is positive and is an increase of the interface between the two layers due to the sliding speed.

When the motion is stopped ($\dot{X} = 0$), after a sliding at low speed ($\dot{X} = 0.2$ nm/s), $T$ does not relax completely (Fig. 5). But, when the movement is stopped ($\dot{X} = 0$), after a sliding at high speed ($\dot{X} = 10^5$ nm/s), $T$ relaxes almost completely.

Film thickness variations $\Delta D$ follow those of friction force variations and can be interpreted as follows.

*(i) The Creep of the Layer.* — During the initial friction process, as shown in Figure 5 or 7, the polymer layer is first sheared at constant thickness $D$ (index $\alpha\beta$ in Fig. 5), then the shear produces a creep of the layer, and therefore a decrease $\Delta D_1$ of the layer, (index $\beta\delta\varepsilon$ in Fig. 5). The absolute value of $\Delta D_1$, is of the same order of magnitude than the size of few monomers size. The decrease of the thickness is probably due to alignment of the polymer chains and may correspond to molecular orientation due to sliding, as already mentionned in the literature [7,39].

*(ii) Film Thickness Variations* $\Delta D_2$. — The $F_s(D)$ curves realised after friction test - not reported here - does not detect any appreciable increase of the adhesive force. Therefore, adhesion of the two compressed adsorbed layers is negligible *before and after* the sliding tests, the shear plane occurs between the two "mesh" layers. Therefore the sliding dissipation is dominated by the small zone at the contact between the two compressed layers, where they "gently" interpenetrate. In these experiments, the direct measurement of the interpenetration zone is not possible. But, the thickness variations $\Delta D_2$, which is an increase of the interface between two layers, is found to be dependent on the sliding speed and is related to the thickness of the interfacial thickness between the two layers.

The absolute value of $\Delta D_2$, is of the same order of the size of a lateral group of the polymer (0.05−0.3 nm, and is small in comparison with the absolute value of creep change $\Delta D_1$. Similar results have been obtained with the friction of "solid" state stearic acid monolayers [12]. In this case the creep change thickness $\Delta D_1$ was negligible (the compressive modulus of stearic acid monolayer is much higher than that of polymer layers studied here), the thickness variations $\Delta D \approx \Delta D_2$ and the thickness increases as the speed increases.

These results suggest that the sliding force $T$, which is dependent on the thickness of the interpenetration zone, is related to the thickness $\Delta D_2$. $T$ decreases when $\Delta D_2$ increases. Therefore, because the sliding process is a dynamic one, it is tempting to relate variations of film thickness $\Delta D_2$, with a characteristic time. The time, $t_a$, it takes one surface to traverse a characteristic polymer dimension such the monomer breath (0.5 nm). Times $t_a$ are found in the range of 10 s to 0.1 ms. As noted (Fig. 5) in the relaxation process after the slow speed test ($\dot{X} = 0.2$ nm/s), molecule groups are more interpenetrated and the tangential force does not relax completely. In opposition, after a step at high speed ($\dot{X} = 10^5$ nm/s, the tangential force relaxes more completely, indicating that chains have less time for interpenetration.

Taking into account Harrison, White, Colton and Brenner *et al.* results [34,35], it is possible to interpret the fluctuations of the thickness $\Delta D_2$ as due to the "levitation", consequence of best trajectories taking by the molecular groups during the sliding. The simulation of the friction of methyl-, ethyl-, and propyl-terminated surfaces placed in sliding contact with an hydrogenated surface, show that, depending on the applied loads, the trajectories of the opposite atoms can differ. For instance, at low loads, the ethyl molecule bends over, lies down and is dragged almost straight across the repulsive potential, like the trajectory a chain would have if one end were tied to the upper surface. At high load, however the ethyl molecule uses its flexibility and length to "snake" (detour) around high potential energy barriers; this trajectory spends less energy and produces a lower friction at higher loads. The friction coefficient for methyl-, ethyl-, and propyl- terminated surfaces is equal to 0.2 and found to be independent of the contact pressure. This value corresponds to the situation where the molecular group snakes.

We think that these simulations explain ours experiments, even if they do not concern explicitly polymers. At high pressure and low speed, the molecular groups use their flexibility to "snake" around the potential barrier and in this case $\Delta D_2$ is small. A pinning state is reached. At high speed, groups are dragged almost in straight line and therefore $\Delta D_2$ is more important.

4.3. Effect of the Contact Pressure. — The compressed layer was characterized with three constant normal load leading to different Hertzian applied pressures $p$: $F_s = 52 \pm 0.3$ $\mu$N, $p = 11$ MPa; $F_s = 508 \pm 1$ $\mu$N, $p = 28$ MPa; $F_s = 2222 \pm 1$ $\mu$N, $p = 49$ MPa. In each experiment, "stabilized" friction forces $T_L$, were detected for each sliding speed. Figure 8 shows the "stabilized" friction coefficient $\mu_L = T_L/F_s$ *versus* the transit time $t_a$. For these three series of experiments, two sliding regimes occur: (i) the "pinning" regime corresponds to $t_a > 0.025$ s or $\dot{X} < 20$ nm/s; in this regime, $\mu_L$ varies with $p$; (ii) the "non-pinning"

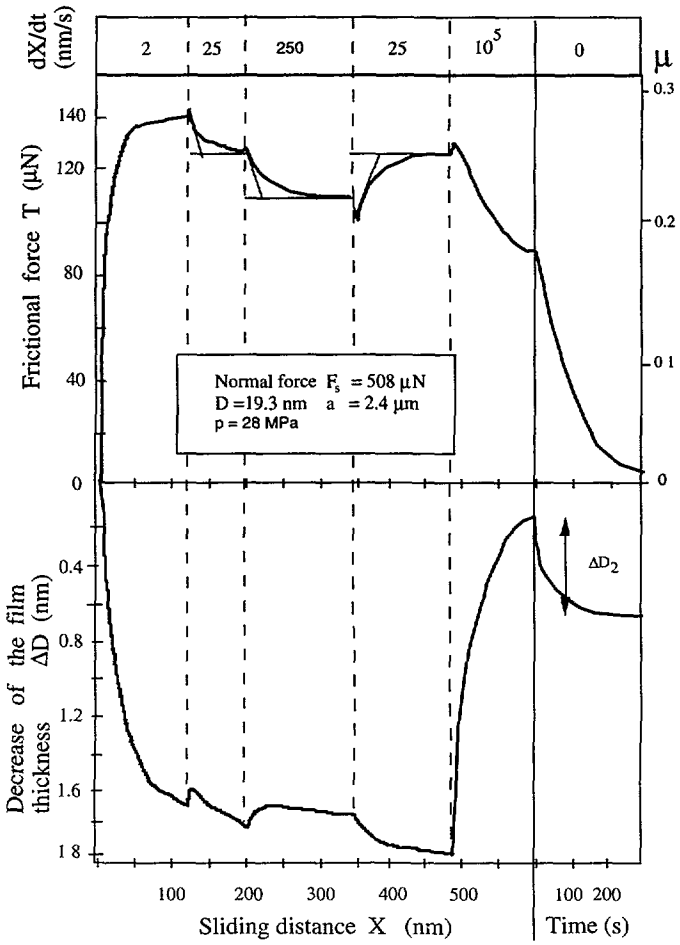


Fig. 8. — Frictional force $T$ and fluctuations of the film thickness $\Delta D$ of the same experiment as in Figure 6, but for different sliding speeds. During the sliding process, the speed is increased by steps (0.1; 2.5; 25; and $10^5$ nm/s).

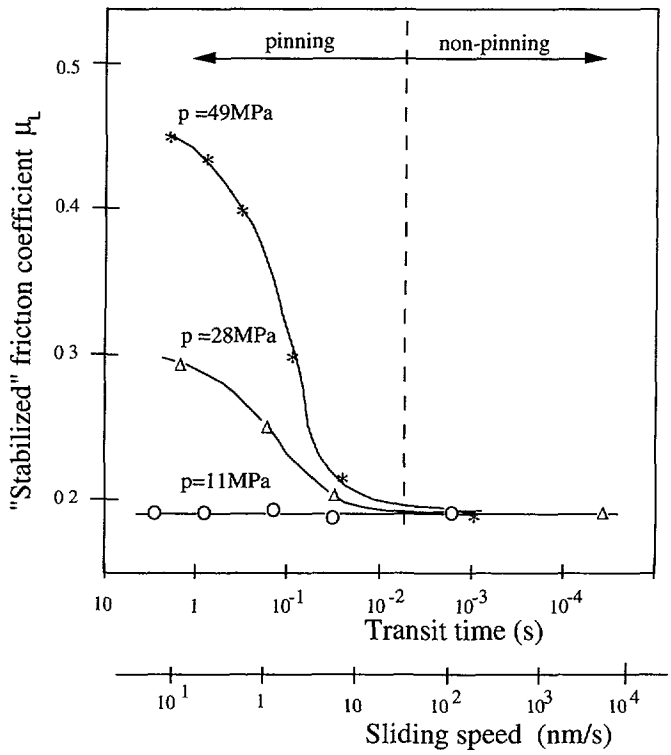


Fig. 9. — Stabilized friction coefficient $\mu_L$, *versus* the transit time. The compressed layer is characterized with three different Hertzian applied pressures $p$. In each experiment, "stabilized" friction forces $T_L$, were detected for each sliding speed.

regime corresponds to $t_a < 0.025$ s, and is characterized by a constant friction coefficient $\mu_L = 0.18 \pm 0.01$. This regime responds to the classical Amonton's law, which is followed when the adhesion is low.

The dissipation of the sliding energy, in the "non-pinning" regime, is due to the vibrations of the groups at a time scale much less than the transit time $t_a$. We expect that the groups flexibility allows their travels in potential energy valleys of the interface. Added to these dissipation energy, in the "pinning" regime another dissipation is founded. It is realised at a transit time of 1 to 10 s, and can correspond to the movement of some monomers. Experimentally, the friction coefficient is found - for high transit time (Fig. 9) - very dependent with the contact pressure. To explain this, the limiting friction coefficient can be written as the following:

$$\mu_L = \mu_{L1} + \mu_{L2} = \frac{T_{L1} + T_{L2}}{F_s} \tag{8}$$

$\mu_{L1}$ and $T_{L1}$ correspond to the end groups contributions acting in both "pinning" and "non-pinning" regimes. $\mu_{L2}$ and $T_{L2}$ correspond to monomer-monomer interactions.

The force $T_{L2}$ can be given as the product of the local force on micro contact times the surface density of micro contact times the surface area:

$$T_{L2} = f\frac{k}{\xi^2}\pi a^2 \tag{9}$$

where $k$ is a constant. If for the compressed layer the entanglement distance $\xi$ is constant:

$$T_{L2} \propto fa^2 \tag{10}$$

According Hertz theory [32], the normal force is:

$$F_s \propto a^3 \tag{11}$$

therefore the friction coefficient is

$$\mu_{L2} \propto \frac{f}{a} \tag{12}$$

But the Hertzian pressure $p$ is proportional to $a$, therefore the friction coefficient is:

$$\mu_{L2} \propto \frac{f}{p} \tag{13}$$

We experimentally found that, at small sliding speed, the stabilised friction coefficient $\mu_{L2}$ is proportional to the pressure $p$, therefore according equation (13),

$$f \propto p^2 \tag{14}$$

But $p$ is also proportional to the squeeze deformation of the layer. Therefore equation (14) suggests that the force $f$ is proportional to the cross section of the part of the molecule in contact.

In conclusion, at low speed interpenetration of the molecules leads to an increase of the friction force and consequently to a shear alignment. These experiments shows that the lowest sliding speed studied leads to the creep of the layer and corresponds to the macroscopic "static" friction [41]. The decrease of the kinetic friction in comparison with the "static" one is found when substantial pression is applied on the contact.

## 5. Conclusions

The following conclusions can be drawn from this study:

(i) Molecularly smooth metal films sputtered on glass surfaces allows the study of the rheology and the friction with a molecular tribometer.

(ii) Nanorheology measurements detect different thicknesses for the polymer adsorbed layers. In the case of cis-polyisoprene in a good solvent, the "hydrodynamic" layer thickness is smaller than the thickness of polymer layer adsorbed on the cobalt surface.

(iii) During the compression process the solvent molecules are repelled from the polymer network. When the separation distance becomes very small, two separated layers of "mesh" polymer are formed.

(iv) The low adhesion found between the two compressed layers permits a definition of the position of the shear plane during the friction test.

(v) During the sliding process the film thickness variation follows the friction force variations and is the sum of two contributions. One is a thickness decrease due to the creep of layers

themselves. Another is an increase of the interface between two layers, found to be dependent on the sliding speed and is related to the interpenetration thickness between the two layers.

(vi) Application of shear results in ordering of the polymer chains that decreases the friction.

(vii) Friction coefficient is found to be dependent on the state of "pinning" of the two "mesh" layers.

**Acknowledgments**

The authors are grateful to A. Schlijper and R. Coy for their helps during the preparation of the manuscript. They are indebted to Shell Research Limited for financial assistance and for providing chemical products. We also thank the French CNRS and all the members of the GDR 936 "mesures des forces de surfaces en milieux liquides", and in particular J.F. Joanny, and J.L. Barrat.

## Appendix A

### Principles of Experiments in Normal Approach

The phenomena taking place at the sphere-plane interface are strongly dependent upon the separation distance between the two surfaces $D$ (Fig. 3b), and this distance depends upon both the approach distance $Z$ between the sphere and the plane, and also the extent of solid deformation $\delta$, giving a true separation $D$ given by

$$D = Z - \delta. \tag{A.1a}$$

The approach distance $Z$ measured from the capacitive displacement sensor, and this origin $Z = 0$ is an electrical one defined from the electrical capacitance $C$ measurements. Indeed, the electrical capacitance $C$ of the sphere-plane interface is expressed as a function of $D$, which is, for negligible solid deformation ($\delta = 0$), identical to the displacement $Z$. It follows, from the expression of the capacitance $C$ as a function of $D$, that the function $(\mathrm{d}Z/\mathrm{d}C)$ is proportional to the separation $D$ between conducting solid surfaces, and thus, the plot $(\mathrm{d}Z/\mathrm{d}C)$ against $Z$ gives the electrical origin $O$ [18]. Consequently, for negligible solid deformation $\delta$, the sphere-plane separation $D$ is, through $Z$, imposed as the superposition of a very low "quasi-static" motion $D_\mathrm{s}$ with a small amplitude harmonic motion (pulsation $\omega$ and amplitude $\tilde{D}$) (Fig. 3c)

$$D = D_\mathrm{s} - \tilde{D}\mathrm{e}^{\jmath\omega t} \tag{A.1b}$$

where $\tilde{D}$ *is small with respect to* $D_\mathrm{s}$, while $D_\mathrm{s}$ changes slowly enough with time to allow neglecting the corresponding velocity $\dot{D}_\mathrm{s}$ with respect to the harmonic component $\omega\tilde{D}$, therefore $D_\mathrm{s}$ will be considered as a constant parameter.

The resulting normal force $F$ can be decomposed into an hydrodynamic component $\tilde{F}_\mathrm{H}$ and a "quasi-static" component $F_\mathrm{s}$ (defined as the force which would subsist in the limit $\tilde{D} \to 0$).

The *dynamic contribution* corresponds to the rheology of the fluid in the interface. For a Newtonian fluid, the hydrodynamic force is given by Reynolds lubrication theory [13,14] and can be written:

$$A = -\frac{F_\mathrm{H}}{\dot{D}} = \frac{\tilde{F}_\mathrm{H}}{i\omega\tilde{D}} = \frac{6\pi\eta R^2}{D} \tag{A.2}$$

It can be noted that, if the viscosity of the fluid $\eta$ and $R$ remain constant, the inverse of the damping function $1/A$ is proportional to $D$. When a polymer is adsorbed irreversibly on the solid surfaces, each surface is covered by a polymer layer of thickness $L$ (Fig. 3b). If the solid

surfaces are separated by distances $D$ large compared with the layer thickness $L$, but small compared with the upper surface radius of curvature $R$, the *dynamic repulsion* is described by Reynolds theory (Eq. (A.2)), after correcting $D$ by a polymer layer "hydrodynamic" thickness $L_H$ [5]:

$$A = -\frac{6\pi\eta R^2}{D - 2L_H} \tag{A.3}$$

$1/A$ function is homogeneous to a length.

The static interactions between the sphere and the plane are first wetting forces created by the liquid meniscus of size comparable to the radius of the sphere, second electrostatic forces produced by the capacitive measurement between surfaces and third surface forces. Experiments are conducted in a such manner that the two first contributions are constant or negligible as function of $Z$ [18].

Therefore, the "quasi-static" normal forces evolutions correspond to interactions between the sphere and the plane, because they are measured at low speed if equilibrium is reached. They correspond to the surface forces $F_S$, created in the vicinity of the contact between the sphere and the plane. For the imposed oscillatory motion, a first order Taylor expansion around $D_s$ gives for this static force

$$F_s = F_s(D_s) - \left[\frac{dF_s}{dD}\right]_{D_s} \tilde{D}e^{i\omega t} \cong F_s(D) - \left[\frac{dF_s}{dD}\right]_{D} \tilde{D}e^{i\omega t} \tag{A.4}$$

showing the contribution of this "quasi-static" force to the harmonic response

$$F_s = F_s(D) - \tilde{F}e^{i\omega t}, \tag{A.5}$$

with $\tilde{F} = \tilde{F}_H + \tilde{F}_s$.

This "quasi-static" contribution includes the local derivative of the static force against distance. This expression is negligible for surfaces far apart, where static forces can be regarded as constant.

The surface force $F_S$ results from solid-solid interactions, which can be attractive or repulsive depending upon the distance $D$ and the nature of the liquid. If the liquid is at thermodynamic equilibrium, this is a truly static intermolecular force. These forces are generally normalised as $F_S/R$ when the substrate contact is not deformed ($\delta = 0$), as proposed by the Derjaguin approximation [21]. Indeed forces carried by the sphere and the plane are related to the interaction energy per unit area $W(D)$ of flat parallel surfaces (a distance $D$ apart), (obeying the same force law as the curved surfaces), by the relation:

$$F_s(D)/R = 2\pi W(D), \tag{A.6}$$

this relation applies for $R \gg D$.

When this "quasi-static" force increases, the elastic deformations of the substrate cannot be neglected any longer. They finally become preponderant so that $D$ may be considered as constant (Fig. 1) The elastic deformations of the substrate can be evaluated, if the interface distance $D$ stays constant, by using the Hertz relation [22]. For a perfectly smooth sphere elastically pressed against a perfectly smooth plane (without any film), total solid deformations are related to the force by:

$$\delta = 0.825 \left(\frac{F_s}{E^*}\right)^{2/3} \left(\frac{1}{R}\right)^{1/3}, \tag{A.7}$$

where $E^*$ is the combined elastic modulus $\frac{1}{E^*} = \frac{1-\nu_1^2}{E_1} + \frac{1-\nu_2^2}{E_2}$; $E_1$ and $E_2$, $\nu_1$ and $\nu_2$ are respectively the elastic modulus and Poisson's ratio of the sphere and the plane, here $E^* = 50$ GPa. The circular Hertzian contact area of radius $a$ is:

$$S = \pi a^2 = \pi R\delta \tag{A.7'}$$

and the computed Hertzian pressure

$$p_{\mathrm{He}} = \frac{F_s}{\pi a^2} = \frac{F_s}{\pi R\delta} \tag{A.7''}$$

In conclusion, simultaneous static and dynamic measurements of normal forces present during the drainage of the sphere-plane interface can characterise the interface.

## References


[1] Briscoe B.J. and Evans D.C.B., *Proc. Roy. Soc. (London)* **A380** (1973) 99-105.

[2] Spikes H.A., Cann P.M., Coy R.C. and Wardle R.W.N., *Lub. Sci.* **3** (1990) 45-62; Cann P.M. and Spikes H.A., STLE/ASME, 93-TC-1B-1 (1993).

[3] Klein J., Kamiyama Y., Yoshizawa H., Israelachvili J.N., Fredrickson G.H., Pincus P. and Fetters L.J., *Macomolecules* **26** (1993) 5552, 5560.

[4] Luckham P. and Klein J., *Macromolecules* **18** (1985) 721, 728.

[5] Fredrickson G.H. and Pincus P., *Langmuir* **7** (1991) 786.

[6] Sens P., Marques C.M. and Joanny J.F., *Macromolecules* **27** (1994) 3812.

[7] Klein J., Perahia D. and Warburg S., *Nature* **352** (1991) 143-145; Klein J., Kumacheva E., Mahalu D., Perahia D. and Fetters L.J., *Nature* **370** (1994) 634.

[8] Yoshizawa H., Chen Y.L. and Israelachvili J.N., *J. Chem. Phys.* **97** (1993) 4128-4140; Yoshizawa H. and Israelachvili J.N., *J. Chem. Phys.* **97** (1993) 11300-11313.

[9] van Alsten J. and Granick S., *Phys. Rev. Lett.* **61** (1988) 2570; *Trib. Trans.* **33** (1990) 436; Carson G.A., Wu H. and Granick S., *Phys. Rev. Lett.* **66** (1991) 2758.

[10] Gee M.L., McGuiggan P., Israelachvili J. and Homola A.M., *J. Chem. Phys.* **93** (1990) 1895-1906.

[11] Homola A.M., Israelachvili J., Gee M.L. and McGuiggan P.J., *Tribology* **111** (1989) 675; *Wear* **136** (1990) 65-83.

[12] Georges J.M., Tonck A. and Mazuyer D., *Wear* **175** (1994) 12, 59-63.

[13] Meyer E., Overney R., Brodbeck D., Howald L., Lüthi R., Frommer J. and Güntherodt H.J., *Phys. Rev. Lett.* **69** (1992) 1777-1780.

[14] Joyce S.A., Thomas R.C., Houston J.E., Michalske T.A. and Crooks R.M., *Phys. Rev. Lett.* **68** (1992) 2790-2793.

[15] Salmeron M.B., *MRS Bull.* **XVIII 5** (1993) 20-25.

[16] Robbins M.O., *MRS Bull.* **XVIII 5** (1993) 45-49; Thompson P.A., Grest G.S. and Robbins M.O., *Phys. Rev. Lett.* **68** (1992) 3448.

[17] Tonck A., Georges J.M. and Loubet J.L., *J. Colloid Inter. Sci.* **126** (1988) 1540-1563.

[18] Georges J.M., Millot S., Loubet J.L. and Tonck A., *J. Chem. Phys.* **98** (1993) 7345-7360.

[19] Wall F.T., *J. Chem. Phys.* **11** (1943) 67; Wagner H.L. and Flory P.J., *J. Am. Chem. Soc.* **74** (1952) 5.

[20] de Gennes P.G., Scaling Concepts in Polymer Physics (Cornell Univ. Press, 1979); Doi M. and Edwards S.F., The Theory of Polymer Dynamics, 1986, Inter. Ser. of Monographs on Physics 73 (Oxford Sci. Publ., 1986).
[21] Israelachvili J.N., Intermolecular and Surface Forces, 2nd Ed. (Academic Press, 1992).
[22] Hertz H.J., *Reine Angew. Math.* **92** (1882) 156.
[23] Cameron A., The principles of Lubrication (J. Wiley, 1967).
[24] Joanny J.F. and Candau S.J., in Comprehensive Polymer Science, C. Booth and C. Price Eds. (Pergamon Press, 1989) p. 199.
[25] Brandrup J. and Immergut E.H., Eds. Polymer Handbook, 2nd Ed. (J. Wiley, 1975).
[26] de Gennes P.G., *Macromolecules* **14** (1981) 1637; **15** (1982) 429.
[27] Pelletier E., Montfort J.P., Loubet J.L., Tonck A. and Georges J.M., *Macromolecules* **28** (1995) 6.
[28] Marques C.M. and Joanny J.F., *J. Phys. France* **49** (1988) 1103.
[29] Rault J., *C.R. Acad. Sci. Paris II* **300** (1985) 433.
[30] Klein J., Kumacheva E., Perahia D., Mahalu D. and Warburg S., *L.J. Faraday Discuss.* **98** (1994) 173-188.
[31] Mindlin R.D., *ASME J. Appl. Mech.* **16** (1949) 289.
[32] Johnson K.L., Contact Mechanics (Cambridge Univ. Press, 1985).
[33] Montfort J.P., Tonck A., Loubet J.L., Georges J.M., *J. Polymer Sci. B* **29** (1991) 677.
[34] Harrison J.A., White C.T., Colton R.J. and Brenner D.W., *Surf. Sci.* **271** (1992) 57.
[35] Harrison J.A., White C.T., Colton R.J. and Brenner D.W., *J. Phys. Chem.* **97** (1993) 6573.
[36] Hirz S.J., Homola A.M., Hadziioannou G. and Frank C.W., *Langmuir* **8** (1992) 328-333.
[37] Briscoe B.J. and Tabor D., *ASLE Trans.* **17** (1978) 158-165.
[38] Briscoe B.J., *Philos. Mag. A* **43** (1981) 511.
[39] Montfort J.P. and Hadziioannou G., *J. Chem. Phys.* **88** (1988) 7187.
[40] Cohen-Stuart M.A., Waajen F.H., Cosgrove T., Vincent B. and Crowley T.L., *Macromolecules* **17** (1984) 1825-15830.
[41] Heslot F., Baumberger T., Perrin B., Caroli B. and Caroli C., *Phys. E* **E49** (1995) 4973.